RECENT DEVELOPMENTS IN MODELING EDDY-CURRENT PROBE-FLAW INTERACTIONS

Harold A. Sabbagh, R. Kim Murphy, Lai Wan Woo, Elias H. Sabbagh
Sabbagh Associates, Inc.
4635 Morningside Drive
Bloomington, IN 47408
and
Kenji Krzywosz
EPRI NDE Center
1300 Harris Blvd
Charlotte, NC 28262

INTRODUCTION

A number of industries have been traditional users of eddy-current technology in nondestructive evaluation (NDE). The traditional mode of eddy-current inspection has been 'monostatic,' in which a single probe is used as both a 'transmitter' and 'receiver.' Research in these industries now indicates the value of using 'bistatic,' or even 'multistatic' probe configurations, in which a single probe is used as a transmitter, and one or more probes are used as receivers. The probes may be either air core, or ferrite core, or perhaps a combination. Some examples of bistatic configurations are the split-core differential probe, and remote-field probes. The industry is turning to computer codes that are based on sophisticated computational electromagnetics algorithms in order to design these probes, and to interpret the signals that arise from the interaction of these probes with flaws.

The volume-integral code, VIC-3D[1] [1], has been enhanced to support the analysis and modeling of multistatic probe configurations, with either air or ferrite cores, and in this paper we report some results of applying this code to several problems. The problems that can be solved include flaws in layered workpieces, that consist of either ferromagnetic or nonmagnetic workpieces.

VOLUME-INTEGRAL EQUATIONS FOR FERROMAGNETIC WORKPIECES

We start with Maxwell's equations

$$\begin{aligned} \nabla \times \mathbf{E} &= -j\omega \mathbf{B} \\ \nabla \times \mathbf{H} &= j\omega \mathbf{D} + \mathbf{J}^{(e)} \ . \end{aligned} \tag{1}$$

Now, $\mathbf{H} = \mathbf{B}/\mu(\mathbf{r}) = \mathbf{B}/\mu_h + \mathbf{B}/\mu(\mathbf{r}) - \mathbf{B}/\mu_h = \mathbf{B}/\mu_h - \mathbf{M}_a$, where μ_h is the host permeability, and $\mathbf{M}_a$ is the anomalous magnetization vector. Thus, the second

[1] VIC-3D is a registered trademark of Sabbagh Associates, Inc.

Review of Progress in Quantitative Nondestructive Evaluation, Vol. 15
Edited by D.O. Thompson and D.E. Chimenti, Plenum Press, New York, 1996

of Maxwell's equations may be written

$$\nabla \times \mathbf{B}/\mu_h = j\omega\mathbf{D} + \mathbf{J}^{(e)} + \nabla \times \mathbf{M}_a \ , \tag{2}$$

which makes clear that the Amperian current, $\mathbf{J}^{(m)} = \nabla \times \mathbf{M}_a$, is an equivalent anomalous electric current that arises because of the departures of the magnetic permeability of the workpiece from the host permeability, μ_h. $\mathbf{J}^{(e)}$, on the other hand, is an electric current that includes the anomalous current that arises due to differences in electrical conductivity; $\mathbf{J}^{(e)} = \sigma_h\mathbf{E} + (\sigma(\mathbf{r}) - \sigma_h)\mathbf{E} = \sigma_h\mathbf{E} + \mathbf{J}_a$. Because the host conductivity and permeability are constant within each plane-parallel layer, they can be accounted for by means of Green functions. This leaves us with only the anomalous electric and magnetic sources to be determined.

In establishing the volume-integral equations, we simply make use of the fact that the total electric field and magnetic flux density at a point is the sum of the fields due to the probe coil, which we call the incident fields, and those due to the anomalous currents, $\mathbf{J}^{(e)}$ and $\mathbf{J}^{(m)}$.

Hence, we write

$$\begin{aligned}
\mathbf{E}^{(i)}(\mathbf{r}) &= \frac{\mathbf{J}^{(e)}(\mathbf{r})}{\sigma_a(\mathbf{r})} - \mathbf{E}^{(0)}(\mathbf{r})\left[\mathbf{J}^{(e)}\right] - \mathbf{E}^{(s)}(\mathbf{r})\left[\mathbf{J}^{(e)}\right] - \mathbf{E}^{(0)}(\mathbf{r})\left[\mathbf{J}^{(m)}\right] - \mathbf{E}^{(s)}(\mathbf{r})\left[\mathbf{J}^{(m)}\right] \\
\mathbf{B}^{(i)}(\mathbf{r}) &= \frac{\mu(\mathbf{r})\mu_h}{\mu(\mathbf{r}) - \mu_h}\mathbf{M}_a + \frac{1}{j\omega}\nabla \times \mathbf{E}^{(0)}(\mathbf{r})\left[\mathbf{J}^{(e)}\right] + \frac{1}{j\omega}\nabla \times \mathbf{E}^{(s)}(\mathbf{r})\left[\mathbf{J}^{(e)}\right] \\
&\quad + \frac{1}{j\omega}\nabla \times \mathbf{E}^{(0)}(\mathbf{r})\left[\mathbf{J}^{(m)}\right] + \frac{1}{j\omega}\nabla \times \mathbf{E}^{(s)}(\mathbf{r})\left[\mathbf{J}^{(m)}\right] \ .
\end{aligned} \tag{3}$$

In arriving at the second equation, we have used the fact that $\mathbf{B} = -(1/j\omega)\nabla \times \mathbf{E}$, and $\mathbf{M}_a = ((\mu(\mathbf{r}) - \mu_h)/\mu(\mathbf{r})\mu_h)\mathbf{B}$.

The first part of the first equation in (3) is the electric-electric (ee) interaction, and the second part is the electric-magnetic (em) interaction. The two parts of the second equation are, respectively, the magnetic-electric (me) and the magnetic-magnetic (mm) interactions. We decompose the various interactions into the 'infinite-space' part, designated by the superscript, (0), and the 'layered-space' part, designated by the superscript, (s). This is done for convenience in coding and problem solving. These interaction operators are expressed as integral operators, with Green function kernels, and are described in more detail in [2].

DISCRETIZATION VIA THE METHOD OF MOMENTS (GALERKIN)

Define a regular grid in three-dimensional space, with grid spacing δx, δy, δz. Relative to this grid we define $\pi(x)$ to be the unit pulse

$$\pi(x) = \begin{cases} 1, & \text{if } 0 \le x \le 1 \\ 0, & \text{otherwise,} \end{cases} \tag{4}$$

and $\pi_{m+1}(x)$ to be the mth-order convolution of $\pi(x)$ (we define $\pi_1(x) = \pi(x)$). The $\pi_{m+1}(x)$ are shown in [3] for $m = 0, 1, 2, 3$.

Next, expand the current vector as

$$\begin{aligned}
J_x(\mathbf{r}) &= \sum_{KLM} J^{(x)}_{KLM} T^{(x)(e)}_{KLM}(\mathbf{r}) \\
J_y(\mathbf{r}) &= \sum_{KLM} J^{(y)}_{KLM} T^{(y)(e)}_{KLM}(\mathbf{r}) \\
J_z(\mathbf{r}) &= \sum_{KLM} J^{(z)}_{KLM} T^{(z)(e)}_{KLM}(\mathbf{r}) \ ;
\end{aligned} \tag{5}$$

the expressions for $T_{klm}^{(q)(e)}$ are:

$$\begin{aligned} T_{klm}^{(x)(e)}(\mathbf{r}) &= \pi_{2k}(x/\delta x)\pi_{1l}(y/\delta y)\pi_{1m}(z/\delta z) \\ T_{klm}^{(y)(e)}(\mathbf{r}) &= \pi_{1k}(x/\delta x)\pi_{2l}(y/\delta y)\pi_{1m}(z/\delta z) \\ T_{klm}^{(z)(e)}(\mathbf{r}) &= \pi_{1k}(x/\delta x)\pi_{1l}(y/\delta y)\pi_{2m}(z/\delta z) \qquad (k,l,m) = (0,0,0),\ldots,(N_x,N_y,N_z) \end{aligned} \quad , (6)$$

where $\pi_{1m}(y/\delta y)$ is the mth unit pulse function, and $\pi_{2k}(x/\delta x)$ is the kth tent function, which is the convolution of $\pi_{1k}(x/\delta x)$ with itself.

The $T^{(q)(e)}(\mathbf{r})$ are called facet elements, because the qth element is constant over the qth facet of the klmth cell. They are used to ensure that the divergence of the current density remains bounded.

Because $\mathbf{J}^{(m)}(\mathbf{r}) = \nabla \times \mathbf{M}_a(\mathbf{r})$, we expand $\mathbf{M}_a(\mathbf{r})$ in edge-elements, which have the required differentiability of the curl operation

$$\begin{aligned} M_x(\mathbf{r}) &= \sum_{KLM} M_{KLM}^{(x)} T_{KLM}^{(x)(m)}(\mathbf{r}) \\ M_y(\mathbf{r}) &= \sum_{KLM} M_{KLM}^{(y)} T_{KLM}^{(y)(m)}(\mathbf{r}) \\ M_z(\mathbf{r}) &= \sum_{KLM} M_{KLM}^{(z)} T_{KLM}^{(z)(m)}(\mathbf{r}) \ , \end{aligned} \tag{7}$$

where

$$\begin{aligned} T_{KLM}^{(x)(m)}(\mathbf{r}) &= \pi_{1K}(x)\pi_{2L}(y)\pi_{2M}(z) \\ T_{KLM}^{(y)(m)}(\mathbf{r}) &= \pi_{2K}(x)\pi_{1L}(y)\pi_{2M}(z) \\ T_{KLM}^{(z)(m)}(\mathbf{r}) &= \pi_{2K}(x)\pi_{2L}(y)\pi_{1M}(z) \ . \end{aligned} \tag{8}$$

These functions are called edge-elements because the expansion coefficient, $M_{KLM}^{(x)}$, is the (constant) value of M_x along the x-directed edge, $(y = (L+1)\delta y, z = (M+1)\delta z)$. There are similar interpretations for $M_{KLM}^{(y)}$ and $M_{KLM}^{(z)}$.

The components of the magnetic current vector are given by

$$\begin{aligned} J_x^{(m)} &= \sum_{KLM} \left[M_{KLM}^{(z)} \pi_{2K}(x)\pi'_{2L}(y)\pi_{1M}(z) - M_{KLM}^{(y)} \pi_{2K}(x)\pi_{1L}(y)\pi'_{2M}(z) \right] \\ J_y^{(m)} &= \sum_{KLM} \left[M_{KLM}^{(x)} \pi_{1K}(x)\pi_{2L}(y)\pi'_{2M}(z) - M_{KLM}^{(z)} \pi'_{2K}(x)\pi_{2L}(y)\pi_{1M}(z) \right] \\ J_z^{(m)} &= \sum_{KLM} \left[M_{KLM}^{(y)} \pi'_{2K}(x)\pi_{1L}(y)\pi_{2M}(z) - M_{KLM}^{(x)} \pi_{1K}(x)\pi'_{2L}(y)\pi_{2M}(z) \right] \ . \end{aligned} \tag{9}$$

We will discretize (3) by employing Galerkin's method, which uses the same vector functions for expansion and testing. The spatial derivatives that could cause problems will be removed by the testing process. Take moments of each of the first three equations of (3) with the corresponding facet element, and of the second three equations with the corresponding edge element. The result for the electric equation is

$$\begin{bmatrix} \mathbf{E}^{(ix)} \\ \mathbf{E}^{(iy)} \\ \mathbf{E}^{(iz)} \end{bmatrix} = \begin{bmatrix} \mathbf{Q}^{(x)} & \mathbf{0} & \mathbf{0} \\ \mathbf{0} & \mathbf{Q}^{(y)} & \mathbf{0} \\ \mathbf{0} & \mathbf{0} & \mathbf{Q}^{(z)} \end{bmatrix}^{(ee)} \begin{bmatrix} \mathbf{J}^{(x)} \\ \mathbf{J}^{(y)} \\ \mathbf{J}^{(z)} \end{bmatrix}$$

$$
+ \begin{bmatrix} \mathbf{G}_{(0)}^{(xx)} & \mathbf{G}_{(0)}^{(xy)} & \mathbf{G}_{(0)}^{(xz)} \\ \mathbf{G}_{(0)}^{(yx)} & \mathbf{G}_{(0)}^{(yy)} & \mathbf{G}_{(0)}^{(yz)} \\ \mathbf{G}_{(0)}^{(zx)} & \mathbf{G}_{(0)}^{(zy)} & \mathbf{G}_{(0)}^{(zz)} \end{bmatrix}^{(ee)} \begin{bmatrix} \mathbf{J}^{(x)} \\ \mathbf{J}^{(y)} \\ \mathbf{J}^{(z)} \end{bmatrix}
$$

$$
+ \begin{bmatrix} \mathbf{G}_{(a)}^{(xx)} & \mathbf{G}_{(a)}^{(xy)} & \mathbf{G}_{(a)}^{(xz)} \\ \mathbf{G}_{(a)}^{(yx)} & \mathbf{G}_{(a)}^{(yy)} & \mathbf{G}_{(a)}^{(yz)} \\ \mathbf{G}_{(a)}^{(zx)} & \mathbf{G}_{(a)}^{(zy)} & \mathbf{G}_{(a)}^{(zz)} \end{bmatrix}^{(ee)} \begin{bmatrix} \mathbf{J}^{(x)} \\ \mathbf{J}^{(y)} \\ \mathbf{J}^{(z)} \end{bmatrix}
$$

$$
+ \begin{bmatrix} \mathbf{G}_{(b)}^{(xx)} & \mathbf{G}_{(b)}^{(xy)} & \mathbf{G}_{(b)}^{(xz)} \\ \mathbf{G}_{(b)}^{(yx)} & \mathbf{G}_{(b)}^{(yy)} & \mathbf{G}_{(b)}^{(yz)} \\ \mathbf{G}_{(b)}^{(zx)} & \mathbf{G}_{(b)}^{(zy)} & \mathbf{G}_{(b)}^{(zz)} \end{bmatrix}^{(ee)} \begin{bmatrix} \mathbf{J}^{(x)} \\ \mathbf{J}^{(y)} \\ \mathbf{J}^{(z)} \end{bmatrix}
$$

$$
+ \begin{bmatrix} \mathbf{G}_{(0)} & \mathbf{G}_{(a)} & \mathbf{G}_{(b)} \end{bmatrix}^{(em)} \begin{bmatrix} \mathbf{M}^{(x)} \\ \mathbf{M}^{(y)} \\ \mathbf{M}^{(z)} \end{bmatrix}, \tag{10}
$$

where the $\mathbf{Q}$'s are tri-diagonal matrices, the $\mathbf{G}_{(0)}$'s the infinite-space matrices, the $\mathbf{G}_{(a)}$'s the convolutional layered-space matrices, and the $\mathbf{G}_{(b)}$'s the correlational layered-space matrices. The infinite-space matrices are convolutional, also. The superscript (ee) denotes electric-electric matrices, and (em) denotes electric-magnetic matrices. The $\mathbf{J}$'s are the unknown electric currents, and the $\mathbf{M}$'s are the unknown magnetic polarization vectors. The last block in (10) is simply a short-hand representation of the three blocks above it, except that it represents electric-magnetic interactions.

The magnetic equation is similar to (10), and is given by

$$
\begin{bmatrix} \mathbf{B}^{(ix)} \\ \mathbf{B}^{(iy)} \\ \mathbf{B}^{(iz)} \end{bmatrix} = \begin{bmatrix} \mathbf{Q}^{(x)} & \mathbf{0} & \mathbf{0} \\ \mathbf{0} & \mathbf{Q}^{(y)} & \mathbf{0} \\ \mathbf{0} & \mathbf{0} & \mathbf{Q}^{(z)} \end{bmatrix}^{(mm)} \begin{bmatrix} \mathbf{M}^{(x)} \\ \mathbf{M}^{(y)} \\ \mathbf{M}^{(z)} \end{bmatrix}
$$

$$
+ \begin{bmatrix} \mathbf{G}_{(0)}^{(xx)} & \mathbf{G}_{(0)}^{(xy)} & \mathbf{G}_{(0)}^{(xz)} \\ \mathbf{G}_{(0)}^{(yx)} & \mathbf{G}_{(0)}^{(yy)} & \mathbf{G}_{(0)}^{(yz)} \\ \mathbf{G}_{(0)}^{(zx)} & \mathbf{G}_{(0)}^{(zy)} & \mathbf{G}_{(0)}^{(zz)} \end{bmatrix}^{(mm)} \begin{bmatrix} \mathbf{M}^{(x)} \\ \mathbf{M}^{(y)} \\ \mathbf{M}^{(z)} \end{bmatrix}
$$

$$
+ \begin{bmatrix} \mathbf{G}_{(a)}^{(xx)} & \mathbf{G}_{(a)}^{(xy)} & \mathbf{G}_{(a)}^{(xz)} \\ \mathbf{G}_{(a)}^{(yx)} & \mathbf{G}_{(a)}^{(yy)} & \mathbf{G}_{(a)}^{(yz)} \\ \mathbf{G}_{(a)}^{(zx)} & \mathbf{G}_{(a)}^{(zy)} & \mathbf{G}_{(a)}^{(zz)} \end{bmatrix}^{(mm)} \begin{bmatrix} \mathbf{M}^{(x)} \\ \mathbf{M}^{(y)} \\ \mathbf{M}^{(z)} \end{bmatrix}
$$

$$
+ \begin{bmatrix} \mathbf{G}_{(b)}^{(xx)} & \mathbf{G}_{(b)}^{(xy)} & \mathbf{G}_{(b)}^{(xz)} \\ \mathbf{G}_{(b)}^{(yx)} & \mathbf{G}_{(b)}^{(yy)} & \mathbf{G}_{(b)}^{(yz)} \\ \mathbf{G}_{(b)}^{(zx)} & \mathbf{G}_{(b)}^{(zy)} & \mathbf{G}_{(b)}^{(zz)} \end{bmatrix}^{(mm)} \begin{bmatrix} \mathbf{M}^{(x)} \\ \mathbf{M}^{(y)} \\ \mathbf{M}^{(z)} \end{bmatrix}
$$

$$
+ \begin{bmatrix} \mathbf{G}_{(0)} & \mathbf{G}_{(a)} & \mathbf{G}_{(b)} \end{bmatrix}^{(me)} \begin{bmatrix} \mathbf{J}^{(x)} \\ \mathbf{J}^{(y)} \\ \mathbf{J}^{(z)} \end{bmatrix}, \tag{11}
$$

where $\mathbf{B}$ is the incident magnetic flux density due to the coil, the superscript (mm) stands for magnetic-magnetic interactions, and (me) stands for magnetic-electric interactions.

The reaction of field, $\mathbf{E}^{(2)}$, on source, $\mathbf{J}_e^{(1)}$, is

$$[1,2] = \int \mathbf{J}_e^{(1)} \cdot \mathbf{E}^{(2)} dV \ . \tag{12}$$

The source with superscript 1 is the primary source due to the exciting coil, and superscript 2 denotes scattered fields (and their sources) due to the flaw. If I_c is the current in the exciting coil, then the change in impedance due to the flaw, as seen by the coil is

$$\Delta Z = -\frac{[1,2]}{I_c^2} = -\frac{[2,1]}{I_c^2} \ , \tag{13}$$

where we have used the reciprocity theorem. If we normalize the excitation to be $I_c = 1$, then

$$\begin{aligned} \Delta Z &= -\int \mathbf{J}_e \cdot \mathbf{E}^{(i)} dV \\ &= -\int (\mathbf{J} + \nabla \times \mathbf{M}) \cdot \mathbf{E}^{(i)} dV \\ &= -\int \mathbf{J} \cdot \mathbf{E}^{(i)} dV - \int \mathbf{M} \cdot \nabla \times \mathbf{E}^{(i)} dV \\ &= -\int \mathbf{J} \cdot \mathbf{E}^{(i)} dV + \int \mathbf{M} \cdot j\omega \mathbf{B}^{(i)} dV \ , \end{aligned} \tag{14}$$

where we have dropped the superscript 2, and replaced the superscript 1 by (i), to denote incident fields. The transference of the curl operator in going from the second to the third equation is valid for $\mathbf{M}$ with finite support.

Upon substituting the expansions for the electric and magnetic solution vectors, (5) and (7), into (14), we get

$$\begin{aligned} \Delta Z = -\sum_{KLM} \Big[& J^{(x)}_{KLM} E^{(ix)}_{KLM} + J^{(y)}_{KLM} E^{(iy)}_{KLM} + J^{(z)}_{KLM} E^{(iz)}_{KLM} \\ & -j\omega \left(M^{(x)}_{KLM} B^{(ix)}_{KLM} + M^{(y)}_{KLM} B^{(iy)}_{KLM} + M^{(z)}_{KLM} B^{(iz)}_{KLM} \right) \Big] \ . \end{aligned} \tag{15}$$

This is a sum of dot-products of the electric current and magnetic polarization solution vectors with the incident electric field and magnetic flux-density vectors.

EXAMPLE: TRANSMIT-RECEIVE COIL CONFIGURATION

Latest eddy current examination methods indicate that more information can be obtained by using a bistatic (or multistatic) configuration, in which a single transmitter excites the workpiece, and one (or more) independent receiver coils detect the signal. Figure 1 shows the classical bistatic arrangement, and the typical probe scanning modes being evaluated with VIC-3D. This arrangement emulates the typical driver-pickup, or transmit-receive (T/R), coil configuration in either normal or parallel scan mode. For the analysis results shown below, both the transmit- and receive-coils were identical 5mm diameter air-core coils with a 10mm separation between the coil centers.

Figure 2 (a) compares the magnitude of the impedance as the probe is scanned in the parallel mode, to the impedance when the probe is scanned in the normal mode.

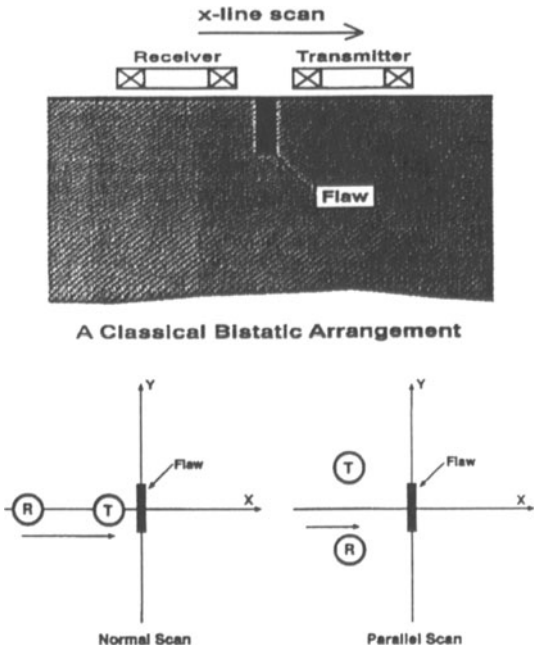

Figure 1: A bistatic arrangement of a typical transmit-receive coil configuration is shown along with the typical scan orientations.

The larger signal in the parallel scan is due to the fact that the transmit-coil induces anomalous currents within the flaw that are virtually parallel to the incident field of the receive-coil (see (12) and (13)). In part (b) of Figure 2, the corresponding impedance plots are displayed as Lissajous patterns, with signal excursions in the opposite directions (upward for the parallel scan, and downward for the normal scan).

It should be noted that the 3mm long notch was centered over the $X - Y$ coordinates of $(0,0)$. Figure 3 shows the actual outputs of a laboratory test, but for a crack that is much larger than the one modeled in Figure 2.

Figure 4 shows a comparison of predicted versus actual outputs from three notches having the same lengths and widths, but with different notch depths. The impedance-plane trajectories at 100 kHz were produced based on the parallel scans using a T/R probe. The model correctly predicts the clock-wise orientation and magnitudes of the impedance-plane trajectories with increasing crack depths.

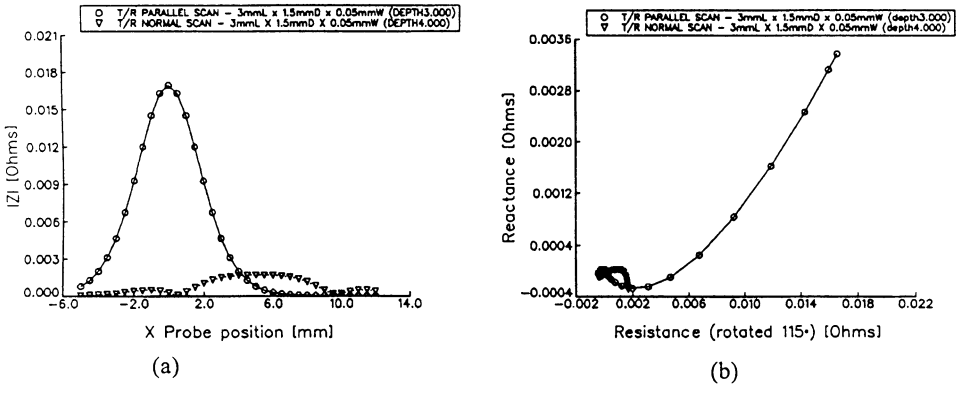

Figure 2: Comparison of signal ouputs shows different results due to normal and parallel scan orientations. The magnitudes are shown in (a), and the impedance plane trajectories are shown in (b).

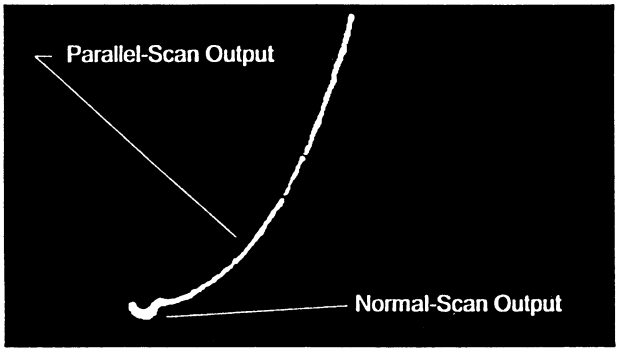

Figure 3: Impedance plane trajectories of two different scan orientations are shown, based on laboratory test results at 100 kHz.

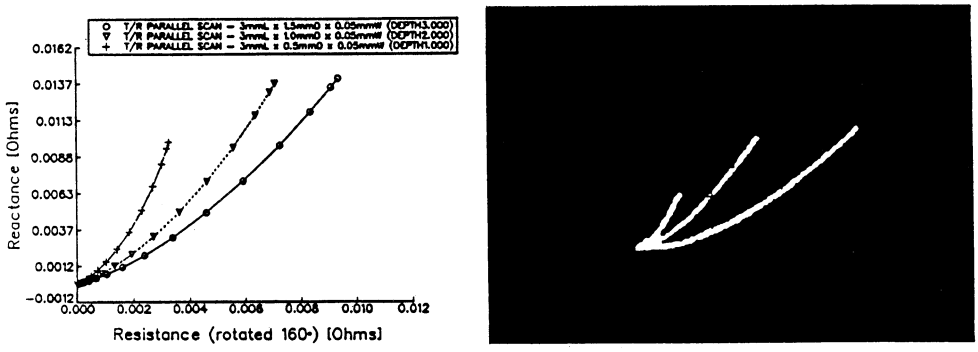

Figure 4: Comparison of predicted and actual outputs for three notches of varying notch depths. The outputs of the T/R probe were obtained at 100 kHz, using parallel scans.

REFERENCES

1. VIC-3D: An Eddy-Current NDE Code User's Guide, Sabbagh Associates, Inc., 4635 Morningside Drive, Bloomington, IN 47408, September 1993.
2. R. K. Murphy, H. A. Sabbagh, J. C. Treece, and L. W. Woo, ''A Volume-Integral Code for Electromagnetic Nondestructive Evaluation,'' Proc. 11th Annual Review of Progress in Applied Computational Electromagnetics, March 1995, pp. 109-116.
3. H. A. Sabbagh, ''Splines and Their Reciprocal-Bases in Volume-Integral Equations,'' IEEE Trans. Magnetics, Vol. 29, No. 6, November 1993, pp. 4142-4152.